Physica Medica 60 (2019) 188–198

Contents lists available at ScienceDirect

Physica Medica

journal homepage: www.elsevier.com/locate/ejmp

Original paper

Imaging biomarker analysis of advanced multiparametric MRI for glioma grading

A. Vamvakas[a], S.C. Williams[b], K. Theodorou[a], E. Kapsalaki[c], K. Fountas[d], C. Kappas[a], K. Vassiou[c], I. Tsougos[a,b,*]

[a] Medical Physics Department, Medical School, University of Thessaly, Larisa, Greece
[b] Neuroimaging Department, IoPPN, King's College London, London, UK
[c] Radiology and Anatomy Department, Medical School, University of Thessaly, Larisa, Greece
[d] Neurosurgery Department, Medical School, University of Thessaly, Larisa, Greece

ARTICLE INFO

Keywords:
Glioma grading
Multiparametric MRI
Radiomics
Machine learning

ABSTRACT

Aims and objectives: To investigate the value of advanced multiparametric MR imaging biomarker analysis based on radiomic features and machine learning classification, in the non-invasive evaluation of tumor heterogeneity towards the differentiation of Low Grade vs. High Grade Gliomas.

Methods and materials: Forty histologically confirmed glioma patients (20 LGG and 20 HGG) who underwent a standard 3T-MRI tumor protocol with conventional (T1 pre/post-contrast, T2-FSE, T2-FLAIR) and advanced techniques (Diffusion Tensor and Perfusion Imaging, 1H-MR Spectroscopy), were included. A semi-automated segmentation technique, based on T1W-C and DTI, was used for tumor core delineation in all available parametric maps. 3D Texture analysis considered 12 Histogram, 11 Co-Occurrence Matrix (GLCM) and 5 Run Length Matrix (GLRLM) features, derived from p, q, MD, FA, T1W-C, T2W-FSE, T2W-FLAIR and raw DSCE data. Along with 1H-MRS metabolic ratios and mean rCBV values, a total of 581 attributes for each subject were obtained. A Support Vector Machine – Recursive Feature Elimination (SVM-RFE) algorithm and SVM classifier were utilized for feature selection and classification, respectively.

Results: Three different SVM classifiers were evaluated with consecutively SVM-RFE feature subsets. Linear SMO classifier demonstrated the highest performance for determining the optimal feature subset. Finally, 21 SVM-RFE top-ranked features were adopted, for training and testing the SMO classifier with leave-one-out cross-validation, achieving 95.5% Accuracy, 95% Sensitivity, 96% Specificity and 95.5% Area Under ROC Curve.

Conclusion: Results demonstrate that quantitative analysis of phenotypic characteristics, based on advanced multiparametric MR neuroimaging data and texture features, utilizing state-of-the-art radiomic analysis methods, can significantly contribute to the pre-treatment glioma grade differentiation.

1. Introduction

Gliomas are the most aggressive primary brain tumors presenting poor survival rates. According to the World Health Organization (WHO) grading system, gliomas are subdivided into four categories considering their malignancy status, i.e. grades I, II (low grade gliomas - LGG) and grades III, IV (high grade gliomas - HGG) [1]. Therefore, preoperative accurate grade classification is of main clinical importance, related to

Abbreviations: Acc, Accuracy; AUC, Area Under Curve; BBB, Blood Brain Barrier; Cho, Choline; cNA, contralateral Normal Area; Cr, Creatine; CSI, Chemical Shift Imaging; DICOM, Digital Imaging and Communications in Medicine; DSCE, Dynamic Susceptibility Contrast Enhanced; DTI, Diffusion Tensor Imaging; DWI, Diffusion Weighted Imaging; FA, Fractional Anisotropy; FLAIR, Fluid Attenuation Inversion Recovery; FSE, Fast Spin-Echo; FOV, Field of View; HGG, High Grade Glioma; IDH, Isocitrate Dehydrogenase; LGG, Low Grade Glioma; LOOCV, Leave-one-out Cross Validation; MD, Mean Diffusivity; mI, Myo-Inositol; MGMT, 6-Methylguanine-DNA Methyltransferase; mp-MRI, multiparametric Magnetic Resonance Imaging; NAA, N-Acetyl Aspartate; NIFTI, Neuroimaging Informatics Technology Initiative; p, Pure Isotropy; PROBE, PROton Brain Exam software; q, Pure Anisotropy; rCBV, relative Cerebral Blood Volume; RGB, Red-Green-Blue color model; ROC, Receiver Operator Characteristic; ROI, Region of Interest; Se, Sensitivity; SNR, Signal to Noise Ratio; Sp, Specificity; SV, Single Voxel; SVM, Support Vector Machine; SVM-RFE, Support Vector Machine - Recursive Feature Elimination; SMO, Sequential Minimal Optimization; VOI, Volume of Interest; WHO, World Health Organization; 1H-MRS, 1H-Magnetic Resonance Spectroscopy; 3T, 3 Tesla; 3D-SPGR, 3-Dimensional Spoiled Gradient Echo

* Corresponding author at: Medical Physics Department, Medical School, University of Thessaly, Larisa, Greece.
E-mail address: tsougos@med.uth.gr (I. Tsougos).

https://doi.org/10.1016/j.ejmp.2019.03.014
Received 3 December 2018; Received in revised form 27 February 2019; Accepted 17 March 2019
Available online 23 March 2019

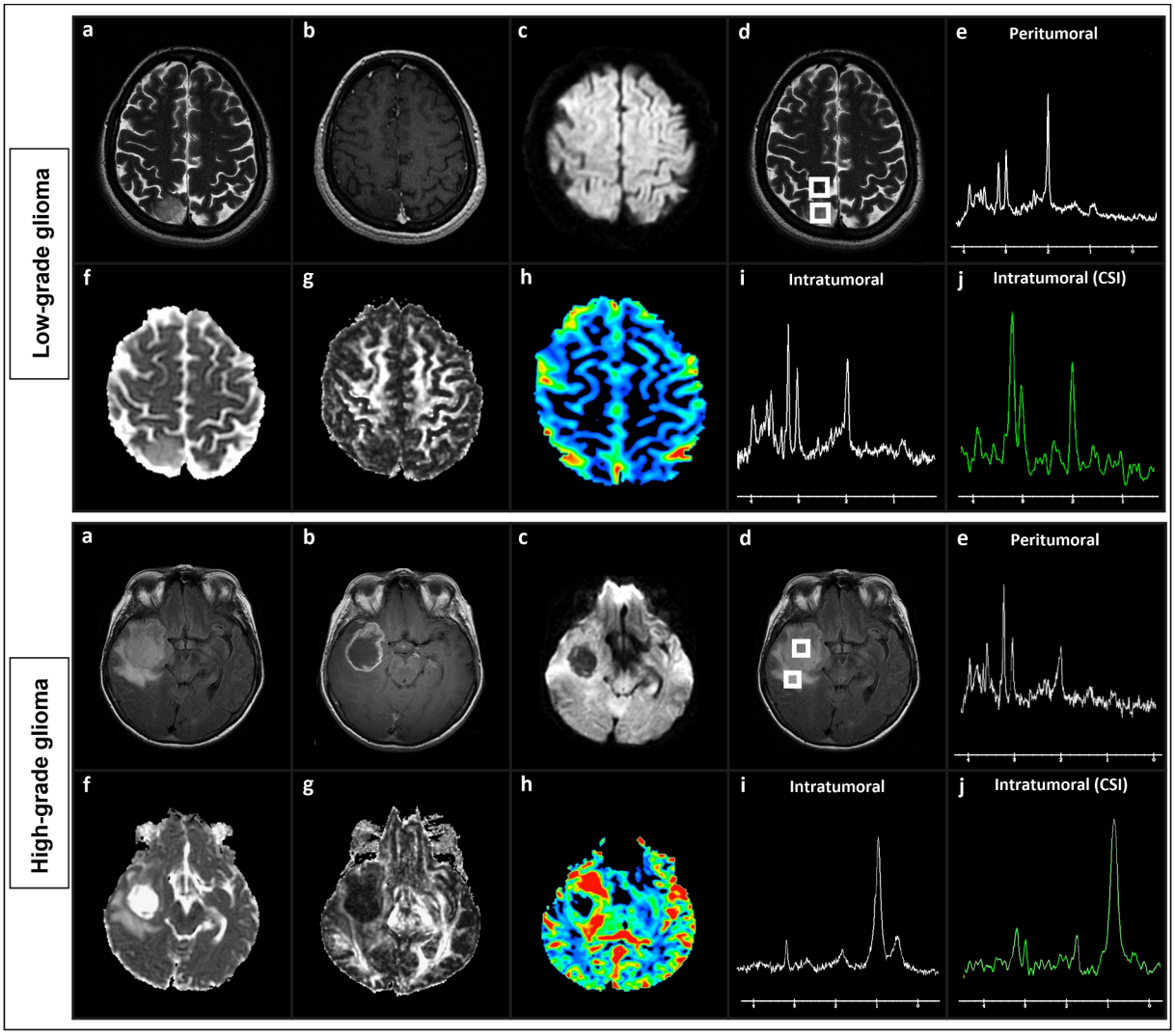

Fig. 1. Upper image; A case of a low-grade glioma, presenting high signal intensity on a T2-weighted image (a), no contrast enhancement on a T1 3D-SPGR image (b) and an isointense signal on a diffusion-weighted image (c). The lesion shows increased MD (f), lower FA (g) and no significant perfusion (h) on the corresponding parametric maps. The peritumoral (e) and intratumoral (i and j) spectra are also depicted. Lower image; A case of a high-grade glioma (glioblastoma multiforme), presenting high signal intensity on a T2-weighted image (a) and ring-shaped enhancement on a T1-weighted post contrast image (b). On the DW-image the lesion presents low signal intensity (c) resulting in higher intratumoral MD (f), lower intratumoral FA (g) and high peritumoral rCBV (h) reflecting tumor infiltration in the surrounding parenchyma. The corresponding peritumoral (e) and intratumoral (i and j) spectra are also depicted.

early prognosis as well as precise selection of the therapeutic approach.

To date, several studies have reported that Magnetic Resonance Imaging (MRI) either with conventional [2–4] or more importantly with advanced MRI sequences [5–8] may contribute in tumor heterogeneity assessment, overcoming sample-biopsy limitations towards glioma grading, providing different perspectives of gliomas pathophysiology. The proposed methods are complemented by advanced image analysis techniques, such as morphological and texture analysis methods, for increasing diagnostic accuracy through the quantitative assessment of the specific information provided by structural and functional MR images [46]. Even though the specific findings seem promising, the increased methodological variability of the current MRI unilateral evaluation approaches, resulting into conflicting sensitivity and specificity reports, could lead to a misinterpretation and hence underestimation of gliomas' biological heterogeneity mechanisms.

As it has been mentioned from certain research studies exploiting multiparametric MRI (mp-MRI) data [9–13], the combination of several MRI parameters, evaluating underlying pathophysiology, may lead to a better understanding of tumor characteristics, and a more accurate classification of LGGs and HGGs. Furthermore, the recent advent of Radiomics i.e. the inclusion of novel approaches incorporating advanced quantification and classification methodologies, which facilitate the manipulation and evaluation of multidimensional imaging feature data, may serve as a sophisticated analysis framework [14,32]. In addition, the potential applicability of radiomic analysis in performing various clinical data associations (e.g. imaging, genomics) [15–16], has been already exploited by some glioma grading studies [17–18], in consent with the 2016 WHO guidelines [19] in which molecular genomic factors (e.g. Isocitrate dehydrogenase (IDH) mutation status, 6-methylguanine-DNA methyltransferase (MGMT) promoter methylation) have been added to histological factors for glioma characterization.

Hence, it is evident that in the precision medicine era, a plethora of quantitative parameters should be taken into consideration for an accurate tumor characterization. In this direction, a radiomic approach with mp-MRI data, can demonstrate a superior contribution towards glioma classification, because of its advantages in describing the detailed microarchitectural and functional tumor processes. However, there is still a demand for further investigation on the validation and utility of combining such techniques, in order to establish a powerful

non-invasive tool in clinical practice [47].

The aim of this study was to create and utilize a radiomic analysis pipeline, to comprehensively evaluate a full 3T multiparametric MRI approach, including all the available advanced techniques, i.e Diffusion Weighted Imaging (DWI), Diffusion Tensor Imaging (DTI), 1H-Magnetic Resonance Spectroscopy (1H-MRS) and Dynamic Susceptibility Contrast Enhanced (DSCE) imaging, in order to produce valid imaging biomarkers for the distinction between high- and low- grade gliomas. The specific implementation utilizes a DTI semi-automated clustering segmentation technique for delineating tumor core Volumes of Interest (VOIs) in all the available MRI parametric images. Radiomic feature extraction included first and second order textural features, and additional advanced MR quantitative parameters (MRS metabolite ratios, relative Cerebral Blood Volume). Feature selection and classification modeling are based on Support Vector Machine classifiers (SVMs), while the discrimination accuracy is evaluated with Receiver Operator Characteristic (ROC) analysis.

To the best of our knowledge, there are only a few studies [20–21] that incorporate conventional MR data accompanied by all the available advanced MR neuroimaging techniques used in brain tumor evaluation. Our approach produced a robust analysis pipeline which shows that radiomic features derived from mp-MRI, supports accurate low vs high grade glioma classification, by exploiting the underlying pathophysiology as expressed by the advanced neuroimaging techniques.

2. Methods and materials

2.1. Multiparametric MRI acquisition protocol

Forty patients initially diagnosed with Low- or High-Grade Gliomas (20 LGG & 20 HGG) underwent an MRI exam on a 3-Tesla MR whole-body scanner (SignaHDx; General Electric (GE) Healthcare, Waukesha, WI, USA), applying an advanced imaging examination protocol including, conventional MRI sequences, 1H-MRS, DWI, DTI and DSCE, using a 4-channel birdcage and an 8-channel phased-array head coil (Fig. 1). Prior to this retrospective study, local Institutional Review Board approval and patient consent was obtained.

The conventional MRI protocol included pre-contrast sagittal and transverse T1-weighted Fast Spin-Echo (FSE) (Repetition Time (TR) / Echo Time (TE) 700 ms/9.3 ms), transverse T2-weighted FSE (TR/TE 2640 ms/102 ms), coronal T2-weighted FSE (TR/TE 2920 ms/102 ms), and T2-weighted Fluid Attenuation Inversion Recovery (FLAIR) (TR/TE 8500 ms/130 ms) scans, with 512 × 512 matrix size, 24 × 24 cm^2 Field of View (FOV), 0.5 mm in-plane resolution and slice thickness of 5 mm with gap 1 mm. Post-contrast isotropic 3-dimensional Spoiled Gradient Echo (3D-SPGR, TR/TE 6.9 ms/2.1 ms, 12 flip angle, 24 × 24 cm^2 FOV, 136 slices of 1 mm thickness and 1 mm^3 voxel size) and T1-weighted post contrast axial images were also obtained.

1H-MRS imaging was performed using the automated PROton Brain Exam (PROBE; General Electric (GE) Healthcare, Waukesha, WI, USA) spectroscopy package before contrast administration to avoid signal disturbance. MRS was performed both as single voxel (SV) and multi-voxel (Chemical Shift Imaging, CSI) when this was feasible. It actually depended on the size of the lesion and the anatomical site. We avoided areas of known susceptibility differences leading to poor field homogeneity, including the mesial anterior temporal and inferior frontal lobes because of their proximity to air-cavities, or proximity to the skull due to lipid contamination. The measurement parameters used in single voxel scans were 1500/35 ms (TR/TE), 128 signal acquisitions and voxel size was chosen to be not less than 3.375 cm^3 for adequate Signal to Noise Ratio (SNR) with a duration of 3 min and 48 sec. The typical single-voxel used was of the order of 8 cm^3 (2 × 2 × 2 cm) for increased SNR. The measurement parameters used in 2D-MRSI were 1000/144 msec (TR/TE), 16x16 phase encoding steps, section thickness ≥ 10 mm and the FOV size was adjusted to each patient's brain anatomy. The duration was of the order of 4 min and 20secs. Typical spectra of the corresponding tumor groups are shown in Fig. 1.

The use of multivoxel (CSI) technique is a very valuable technique to evaluate simultaneously the retrospective area of the tumor site (when applicable, taking into account areas of heterogeneity and lipids contamination), and was acquired at a higher echo time of 144 ms hence we had a better evaluation of lipids and lactate. The differentiation of Lipids and lactate when in doubt was done using the flipping of lactate at long TE (144 ms) and analysis using the TARQUIN software (http://tarquin.sourceforge.net/) [22].

We generally used the auto shimming method based on the vendor's software, but manual shimming was implemented in difficult cases by adjusting receiver/transmitter gains. There were a few times that despite all this effort, complete elimination of small local deviations from the B0 field uniformity was very difficult and these cases were omitted. In general, our linewidth was kept below 10 hz for SV and below 20 hz for CSI.

Diffusion-weighted MR imaging was performed prior to contrast media injection, via a single-shot, spin-echo, echo planar sequence with b-values of 0 s/mm^2 and 1000 s/mm^2 performed in 50 sec. DTI was performed in the axial plane with single-shot spin-echo echo planar: TR/TE 8000 ms/89.8 ms, gradients applied in 32 non-linear directions, b = 0 s/mm^2 and 1000 s/mm2, FOV = 24 cm^2, 1 mm in-plane resolution, slice thickness = 4 mm with gap = 1 mm and NEX = 1, with a duration of 4 min and 32sec.

The DSCE MR images were acquired with a single-shot gradient echo planar imaging sequence (TR/TE 2000 ms/20.7 ms, flip angle 60°, FOV = 24 × 24cm^2, slice thickness = 5 mm with gap = 1 mm, NEX = 1) during the first pass of bolus of gadolinium contrast material (DOTAREM) at a dose of 0.1 mmol/kg body weight with a duration of 1 min and 08 sec. The location of the perfusion-weighted MR data set was determined by using the axial T1-weighted images after contrast injection to locate the lesion and axial T2-weighted images to locate the peritumoral T2 signal abnormality.

At this point it has to be mentioned that gadolinium-containing contrast agents are normally excluded by the blood-brain barrier (BBB) and cannot enter the extracellular spaces of the brain and spinal cord. The disruption of the BBB caused by diseases like enhancing tumors, subacute infarcts etc., results in leakage of the contrast agent into the extravascular space. This leakage should be corrected for, because it can lead to systematic errors due to the additional pronounced T1- and T2*-relaxation effects that violate the fundamental assumption of tracer kinetic modelling on which DSCE is based, that no recirculation of the contrast agent occurs. Hence T1 shortening from extravascular gadolinium can lead to increased signal and may blunt the desired T2* shortening on which DSCE is based on. Several strategies exist to minimize this effect, from simple techniques to more sophisticated models of the first pass kinetics [23–24]. One simple and popular method that we have used in our work is called 'preloading'. A one-fourth to one-third of the total dose was administered about 5–10 min before the dynamic imaging, and a T1 weighted to guide the perfusion section positioning was run in between. This 'preloading' of gadolinium reduces contaminating T1 effects by shortening the pre-bolus intravoxel T1, raising the baseline signal so that T2* changes can then be better appreciated [25].

2.2. Data post-processing

Initially, all available MRI raw data were converted from Digital Imaging and Communications in Medicine (DICOM) to Neuroimaging Informatics Technology Initiative (NIFTI) 1.1 format with the 'dicom2nii' tool provided by MRIcron software (https://www.nitrc.org/projects/mricron). Subsequently, FSL software of FMRIB Software Library v5.0 (fsl.fmrib.ox.ac.uk/) [26–28], was utilized for parametric MR volumes co-registering and re-slicing into an isotropic voxel size of 1 mm^3, as well as applying bias field corrections. DTI data post-processing was performed with FSL, including motion artifacts and eddy

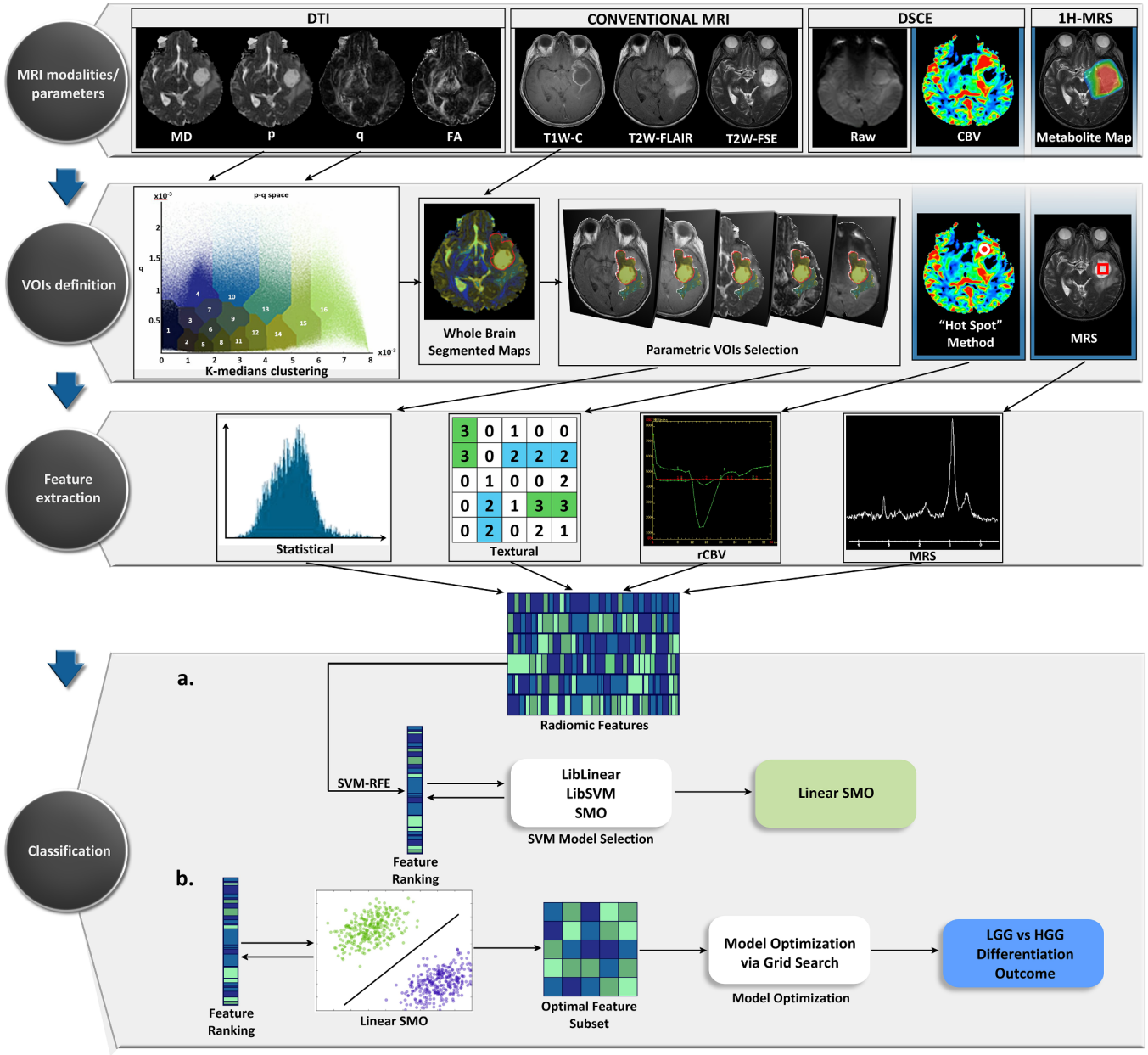

Fig. 2. The Radiomic Analysis pipeline of the study. In the first two sub-panels a complete sample of a patient's multiparametric MR images and the respective VOIs placement methodologies are depicted. Subsequently, the figure presents feature extraction (third sub-panel) and the two steps of classification (fourth sub-panel), including (a) the optimal SVM classifier selection and (b) the optimal feature subset definition, along with the final differentiation outcome.

current distortions corrections [29], brain tissue extraction, Diffusion Tensor estimation and Mean Diffusivity (MD), Fractional Anisotropy (FA), Pure Isotropy (p) and Pure Anisotropy (q) parametric maps calculation [30]. In-vivo SV and multivoxel spectroscopic data analysis and calculation of metabolite ratios were performed on an Advanced Linux workstation using the Functool software (GE Healthcare). Post-processing of the raw spectral data included baseline correction, frequency inversion and phase shift. Gaussian curves were fitted to N-Acetyl Aspartate (NAA), Choline (Cho), Creatine (Cr), lipid and lactate metabolites' peaks for determination of peak area. Finally, metabolite ratios of NAA/Cr, Cho/Cr, mI/Cr and Lipids/Cr were calculated from the area under each metabolite peak. The Functool software was utilized for processing DSCE data and analyzing the perfusion imaging time curves for extracting the Cerebral Blood Volume (CBV) parametric maps. In addition, the gadolinium uptake time curves were also utilized for identifying the volume of contrast agent maximum uptake for every patient, which was used in the subsequent radiomic analysis process for textural features extraction (Fig. 2).

2.3 Volume. of interest (VOI) extraction

In the framework of radiomic-based quantification of tissue heterogeneity, the accurate and reproducible segmentation of regions and volumes of interest is critical. To this scope, a clustering segmentation method reported in a previous study by Vamvakas et al. [31], was utilized for the identification of different tumor subregions (habitat imaging [32]), providing the radiologist with the appropriate information for manually performing whole tumor delineation. However, the quantification of tumor imaging characteristics may easily be biased from the presence of peritumoral edema and hemorrhagic tumor components, which don't have a contiguous occurrence in the two tumor groups. Probably, they would be offered as semantic annotations

[32], however semantic features were not considered in this study.

In the literature both intra and peritumoral regions are usually evaluated [33–35]. The hypothesis is that high grade gliomas are infiltrative lesions, thus pathological tissues may be present in the surrounding white matter, while low grade gliomas are not. Therefore, the surrounding edema of LGGs is considered to be pure vasogenic whereas around HGGs there should be a combination of vasogenic edema and infiltrating tumor cells along the perivascular spaces. Hence all techniques would yield some kind of differentiation based on that. On the other hand, a great deal of evidence in the literature supports that there can be great discrepancies regarding the peritumoral region especially regarding MRS and DTI [12,36,37]. Moreover, LGGs often appear without any significant peritumoral parenchyma alteration, hence a reproducible estimation would be to compare the actual tumors and evaluate whether radiomic techniques such as texture or morphological features may provide extra information. Therefore, we opted to evaluate only the intratumoral area, aiming to identify differences regarding diffusive and solid growth patterns of LGGs and HGGs respectively, for two reasons: a) The radiomic analysis regarding textural features should be performed on a directly comparable and reproducible evaluation area for both tumor types. Hence in order to ensure lack of bias and reproducibility we chose to use the tumor core of both lesions, and b) there can be difficult cases where peritumoral evaluation might not be possible, either due to areas of poor homogeneity (e.g. air filled cavities like the sinuses or proximity to the skull) or maybe even to the lack of cooperation of the patient for the whole duration of the exam (especially for MRS). In such cases, the radiologist is left with the evaluation of the intratumoral area which is obtained first. So the hypothesis is that an evaluation of the intratumoral region only, should be able to discriminate between tumor grades.

The proposed clustering segmentation method is based on DTI parametric maps for classifying the brain voxels of each patient into groups with similar isotropic and anisotropic diffusion properties, accounting for normal and tumorous brain tissue diffusivities. Specifically, k-medians clustering (k = 16) is applied on a 2D histogram of p (isotropic) and q (anisotropic) components of the diffusion tensor, derived from all patient cohort. Subsequently, Red-Green-Blue (RGB) color mapping of clusters according to the relative magnitudes of p, q and T2 (from b = 0 s/mm^2 DTI volumes) values of the cluster centroids and subsequent color assigning to each individual patient's brain voxels according to their position in the p-q space, results in whole brain segmented maps (Fig. 3). These color-coded maps are based on the contouring provided by diffusion properties, being robust in displaying tissue microarchitecture, thus healthy and tumorous brain tissues present distinctive boundaries.

Finally, tumor core segments highlighted by the clustering technique, were delineated on colormaps by an experienced radiologist, and stacked up to form tumor VOI masks. Subsequently, these VOI masks where applied on the various co-registered multiparametric images of our dataset (Fig. 2), resulting in a set of 3D parametric representations of the gliomas.

Each patient's VOIs taken into account were exactly the same on every tumor core region for all the imaging series (i.e. T1, T2, FLAIR, DTI and DSCE raw) except for CBV and spectroscopy. Specifically, the rCBV measurements were calculated from ROIs which were placed in regions of the highest perfusion as seen on the CBV color overlay maps, referred as the 'hot spot' method. The placement of ROIs was carefully performed to avoid large vessels based on the combined information from T1-weighted image after contrast enhancement, and T2-weighted FSE images. The mean rCBV was used for the subsequent analysis.

For both spectroscopic techniques, a rectangular ROI was localized by using the transverse T2-weighted FLAIR or T2-weighted FSE, sagittal T1-weighted FSE and coronal T2-weighted FSE imaging sequences. Spectra for each patient were acquired from the intratumoral, peritumoral and contralateral regions of interest. The contralateral Normal Area (cNA) was used as the control spectrum. Within the tumor, the size and location of the voxel were carefully adjusted to include as much of the solid tumor portion as possible, avoiding the inclusion of obvious cyst, hemorrhage, edema, calcification, and normal-appearing brain. For each patient, the SV scan was first applied in the intratumoral region of interest followed by peritumoral and cNA. The 2D-MRSI scan was then performed, including the region as the one previously chosen for the SV scan, in order to have a direct metabolite comparison between the two 1H-MRS techniques.

2.4. Radiomic feature extraction

Histogram analysis have considered 12 statistical features (Appendix A.1–12) acquired from normalized data histograms with an in-house MATLAB 2015b (https://www.mathworks.com/) code. Texture analysis was implemented in MaZda ver.5 software (http://www.eletel.p.lodz.pl/programy/mazda/) [38–40], considering 11 Gray-Level Co-Occurrence Matrix-based (GLCM) in 5 pixel distances and 5 Gray-Level Run Length Matrix-based features (GLRLM), both calculated on 8-bit quantized images. After the acquisition, textural features (Appendices B.1–11 and C.1–5), were averaged over the 13 directions of the 3D image, to obtain directionality independence measurements. In summary, the quantitative radiomic features extracted from the eight tumor parametric VOIs, regarding p, q, MD, FA, T1W-C, T2W-FSE, T2W-FLAIR and volumes of maximum gadolinium uptake of DSCE MRI, along with the four metabolic ratios of 1H-MRS (Ch/Cr, NAA/Cr, mI/Cr, Lipids/Cr) and mean rCBV values (Fig. 2), resulted in a total of 581 distinct attributes for each subject.

2.5. Feature selection and classification

In a recently reported study, Zhang et al. [41] have made comparisons between several feature selection and classification algorithms implemented in Weka software (https://www.cs.waikato.ac.nz/ml/weka/) [42], regarding a mp-MR dataset for glioma grade classification. According to their results, the combination of Support Vector Machine – Recursive Feature Elimination (SVM-RFE) and SVM classification demonstrated superior performance regarding the specific task, in comparison with other feature selection and classification models.

Adopting the indices and the basic methodological concepts of the abovementioned study, machine learning feature selection and classification were implemented in Weka 3.8 software, following four major steps, as they are described below (Fig. 2):

In the beginning, radiomic features were imported in the SVM-RFE algorithm ('SVMattributeEval' with the 'Ranker' search method), which is a wrapping feature selection method introduced by Guyon et al. [43]. More specifically, SVM-RFE iteratively eliminates a set of features by removing the less important one, according to the weighting vectors of an SVM classifier. Consequently, feature ranking in a descending order of discriminative importance is obtained, according to the elimination sequence.

Afterwards, the performances of different well established SVM packages ('LibLinear', 'LibSVM', 'SMO') were evaluated with Receiver Operator Characteristic (ROC) analysis, on consecutively SVM-RFE feature subsets, to identify the SVM model presenting the best fitting to our dataset. Each classifier was repeatedly trained, starting with the 10 higher-ranked features with a stepwise of adding up 10 features at each iteration, and tested with leave-one-out cross-validation (LOOCV) to avoid overfitting by increasing the number of folds. As it was observed, the 'SMO' package with linear kernel (default), that is an SVM classifier implementing Platt et al. Sequential Minimal Optimization (SMO) algorithm [44], achieved the best performance, compared to 'LibLinear' and 'LibSVM'. At this step, all the above-mentioned SVM classification packages were implemented utilizing Weka 3.8 default hyperparameters.

Subsequently, the task of determining the optimal feature subset was driven by the classification performance of 'SMO' classifier through

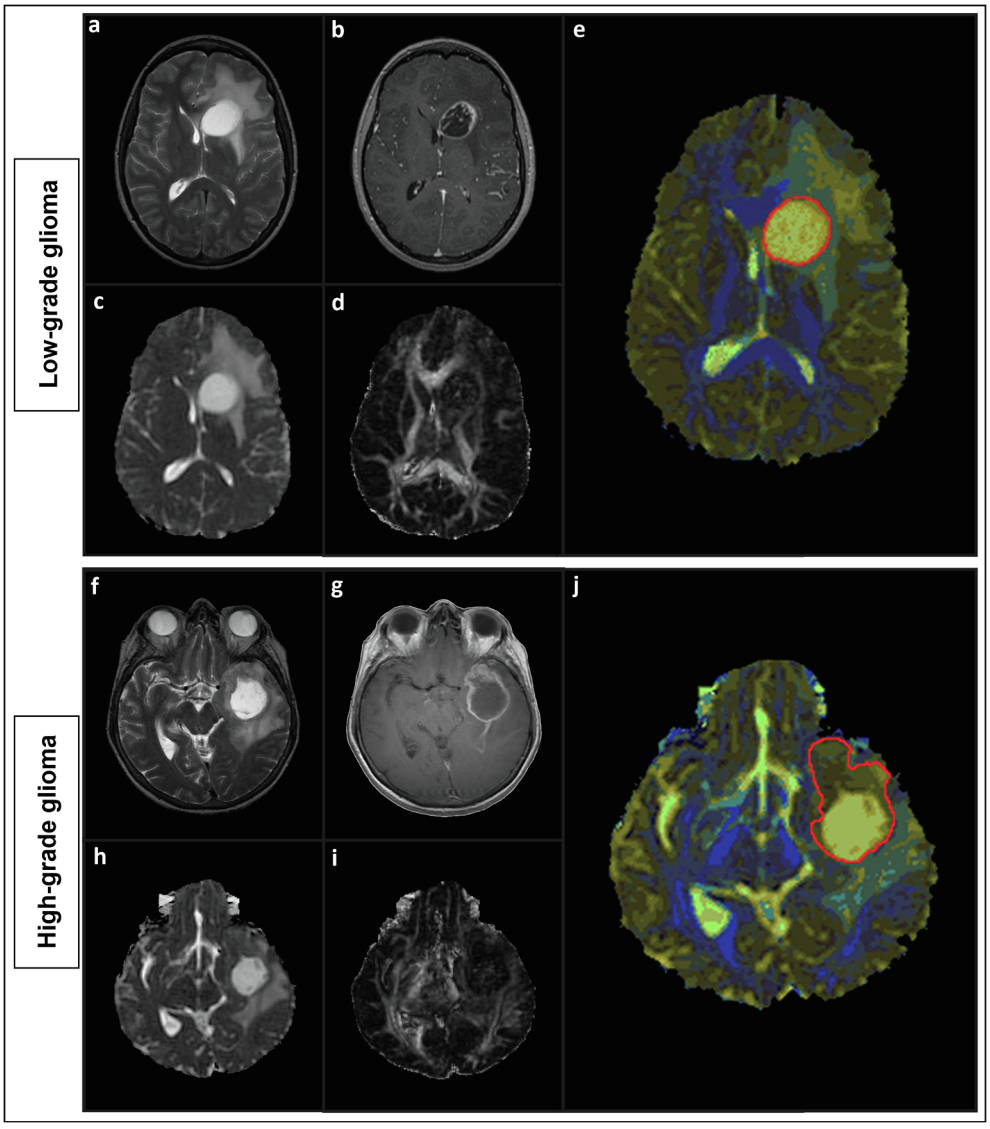

Fig. 3. Whole brain segmented maps of a LGG (e) and a HGG (j) case, resulting from the k-medians clustering of the DTI isotropic (c, h), anisotropic (d, i) and T2-wheighted components feature space (a, f). The different colors presented (k = 16) correspond to distinct brain tissue diffusion properties, which facilitate the precise definition of healthy tissue, tumor core and peritumoral edema. The final delineation of tumor core (red outline) is the outcome of the further combination with T1-wheighted post-contrast imaging (b, g).

a detailed investigation between different numbers of SVM-RFE top ranked features, with a stepwise of adding 1 feature at each iteration.

As soon as the optimal features where determined, according to the subset presenting the highest accuracy values, further investigation through a grid search method ('GridSearch') aiming in accuracy maximization was utilized for optimizing the hyperparameters of the classification model.

At this point, it should be noted that all data post-processing and analysis steps were implemented in state-of-the-art software which have been utilized by many studies [55]. In addition, the results of our work have been based on the pre-validations of the used software, as these were analytically described in their original studies [22,26–30,38–40,42].

3. Results

The initial classification trials performed in the study have shown that linear kernel 'SMO' algorithm demonstrated better classification performance (Acc = 90%/AUC = 0.899) in comparison with 'LibLinear' (Acc = 55%/AUC = 0.500) and 'LibSVM' (Acc = 75%/AUC = 0.732). The subsequent evaluation of different feature subsets with linear 'SMO', has nominated the adaptation of 21 SVM-RFE top ranked features, shown in Table 1, which provide the highest discriminating ability between LGGs and HGGs (Acc = 95%/Se = 93.9%/Sp = 94.4%/AUC = 94.4%). Also, Lipids/Cr metabolic ratio was the highest ranked feature. As shown in Table 2, all MRI modalities/parameters have contributed in the final feature set, except for DTI's Fractional Anisotropy (FA). In addition, 8 features where histogram-based and 12 features where textural-based, while GLCM features were much more statistically significant than GLRLM (11vs1).

Finally, the classification model refinement performed by 'Grid Search' method, have determined a complexity parameter $c = 10^3$ for the linear kernel 'SMO', demonstrating a total performance of 95.5% Accuracy, 95% Sensitivity, 96% Specificity and 95.5% Area Under the ROC Curve.

4. Discussion

In the present study, radiomic analysis on a 3T mp-MRI dataset was performed for the classification between low- and high-grade gliomas.

Table 1
SVM-RFE top-ranked feature subset selected for classification.

Rank	MRI modality/parameter	Quantification Method	Radiomic Feature	LGG mean ± sd	HGG mean ± sd
1	1H-MRS	–	Lipids/Cr	0.90 ± 0.38	3.34 ± 1.17
2	T1W-C	Histogram	Skewness	0.17 ± 0.79	0.56 ± 0.21
3	q	Histogram	Mean	0.32 ± 0.07 *	0.24 ± 0.05 *
4	T1W-C	Histogram	Variance	211.91 ± 38.59	402.46 ± 64.09
5	MD	GLCM	Inverse Difference Moment	0.16 ± 0.05	0.11 ± 0.04
6	q	GLCM	Sum of Squares	115.91 ± 19.98	133.73 ± 15.62
7	DSCE	GLRLM	Run Length Non-Uniformity	904.61 ± 460.26	1901.95 ± 1046.79
8	T1W-C	GLCM	Angular Second Moment	2.48 ± 0.90 **	1.79 ± 0.30 **
9	T2W-FLAIR	GLCM	Difference Variance	47.98 ± 27.73	23.51 ± 11.68
10	q	GLCM	Correlation	0.24 ± 0.10	0.17 ± 0.16
11	q	Histogram	Median	0.29 ± 0.06 *	0.22 ± 0.04 *
12	MD	GLCM	Difference Entropy	1.23 ± 0.11	1.35 ± 0.10
13	T2W-FLAIR	Histogram	Variance	174.33 ± 33.33	140.05 ± 36.21
14	rCBV	–	Mean	1.68 ± 0.59	6.80 ± 4.13
15	p	GLCM	Contrast	94.79 ± 51.75	156.34 ± 63.78
16	T2W-FLAIR	GLCM	Sum Variance	171.32 ± 76.73	102.79 ± 37.33
17	DSCE	Histogram	Minimum	0.29 ± 0.11	0.22 ± 0.10
18	T2W-FLAIR	GLCM	Difference Entropy	1.25 ± 0.11	1.19 ± 0.10
19	T2W-FSE	Histogram	Entropy	5.15 ± 0.39	4.94 ± 0.36
20	DSCE	GLCM	Angular Second Moment	4.97 ± 2.89 **	2.40 ± 1.38 **
21	q	GLCM	GLCM Sum Entropy	1.79 ± 0.05	1.76 ± 0.05

*Mean and Standard error in the units $x10^{-3}$ mm^2/s
**Mean and Standard error in the units $x10^{-3}$

The specific implementation utilized a semi-automated clustering segmentation technique for delineating tumor core VOIs in all available MR parametric volumes, derived from structural MRI sequences (T1W-C, T2W-FSE, T2W-FLAIR), Diffusion Tensor Imaging (p, q, MD, FA,) and Dynamic Susceptibility Contrast Enhanced MRI raw data (maximum gadolinium uptake volumes). Subsequently, several quantitative histogram and textural features were calculated on each patient's parametric VOIs. Additional MRS metabolic ratios (NAA/Cr, Cho/Cr, mI/Cr and Lipids/Cr) and mean rCBV values, extracted from corresponding tumor VOIs, were considered, finally forming a set of 581 quantitative parameters (features) for each individual patient, which were inserted into the SVM-RFE in order to acquire feature ranking in a descending order of discriminative importance. Subsequently, comparisons performed between different SVM classifier implementations resulted in the adoptation of linear kernel SMO classifier as the more efficient classification performance on our data set. The classification model utilizing 21 mp-MRI radiomic features, demonstrated 95.5% Accuracy, 95% Sensitivity, 96% Specificity and 95.5% Area Under ROC Curve in differentiating LGG vs HGG.

The justification for implementing the specific SVM feature selection and classification methods on our mp-MRI dataset, is based on the predictive robustness indicated by similar studies regarding glioma grading in the past. In a computer-aided-diagnostic approach, Chen et al. [45] utilized SVM-RFE for selecting textural features, derived from CNN-based segments which were based on conventional MRI data only, and XGBoost classification, presenting a 91.27% accuracy. On the other hand, Citak-Er et al. [20] have proposed a sophisticated SVM-RFE implementation, in which different tumor ROIs mean values were analyzed with the addition of advanced techniques (MRS, DSCE) but without a texture analysis approach as in our work. Their results utilizing the SVM-RFE outcome for training a linear SVM classifier yielded 93% classification accuracy. More importantly, Tian et al. [21] in a very recent study (2018), following their initial approach [41], proposed a multi parametric, MRI glioma grading classification scheme including advanced techniques such as Arterial Spin Labelling (ASL) perfusion imaging, which was based on SVM-RFE and RBF kernelized SVM. Contrary to Citak-Er et al. [20], they have utilized a texture analysis approach similar to ours, showing 96% accuracy and 98% AUC values. Hence, it is evident that the addition of advanced MRI techniques and multiparametric texture analysis data, substantially improves the classification performance. In fact, when applying the same classification procedure in this data set, excluding the advanced quantitative parameters the performance dropped to 90% Accuracy, 90% Sensitivity, 97% Specificity and 89% AUC.

Even though Tian's et al. [21] study presents slightly better performance outcomes compared to our study, our model utilizes a significantly smaller number of radiomic features imported into the SVM classifier (21 vs. 28), increasing its relative efficiency. Since the two studies follow similar feature extraction, selection and classification methodologies, it is obvious that our study's good performance should be attributed to the addition of the micro-architectural and metabolic neuroimaging data utilized, i.e. Diffusion Tensor and Spectroscopic imaging, not included in Tian's et al. study. As it is depicted in table 1, in our study an important number of features extracted from these techniques, have shown high discriminative ability, as this is already investigated and confirmed in previous studies [12,48].

More specifically DTI and MRS as additional quantitative parameters have already proven their ability in conventional analysis

Table 2
Summarized results showing the distribution of the significant radiomic features among MR modality/parameter and feature extraction method.

MRI modality/parameter											
Features		Conventional MRI			DTI				DSCE		MRS
		T1W-C	T2W-FSE	T2W-Flair	MD	FA	p	q	Raw	rCBV	Lipids/Cr
Histogram		2	1	1	0	0	0	2	1	–	–
Textural	GLCM	1	0	3	2	0	1	3	1		
	GLRLM	0	0	0	0	0	0	0	1		
Total Radiomic Features		**3**	**1**	**4**	**2**	**0**	**1**	**5**	**3**	**1**	**1**

techniques. Regarding diffusion imaging, several previous studies have reported the value of textural features of Apparent Diffusion Coefficient (ADC) maps as potential biomarkers for glioma grade differentiation [5–6,49–50]. In a more recent study, Raja et al. [51] investigated the contribution of Diffusion Tensor and Diffusion Kurtosis Imaging in grading of gliomas. Their texture-based features have shown significant differences regarding several DTI parametric maps, except for FA, which comes in agreement with the results of our study. However, we have found that the anisotropic diffusion tensor component, as expressed by the pure anisotropy parameter (q) has proven to be of great importance (5 out of the 21 features were derived for q maps) and could play an essential role in glioma heterogeneity assessment.

In addition to DTI, MR spectroscopy is a powerful technique for evaluating brain tumor metabolic processes with an increased diagnostic impact. Many studies support the potential of MRS metabolic ratios in glioma grade differentiation [8–10,52], especially when combined with other advanced techniques. Even though a statistically significant difference for the specific ratios was not observed in our study, which might be expected since we are comparing HGGs vs LGGs [53], however the MRS derived Lipids/Cr ratio was the highest ranked feature compared to the total number of the radiomic features utilized. Consequently, the lipids concentration in glioma's tumor core, which is proportional to the extent of tumor's necrotic component, may serve as a robust imaging biomarker in differentiating between Low- and High-grade gliomas.

Perfusion imaging has evolved to a clinical tool of high importance in characterizing tumor malignancy status due to its increased correlation with cancer proliferation and progression. As shown in Table 2 a significant number of features imported to the classification model (7 out 21), are derived from perfusion MR techniques. These results come in agreement with previously reported studies [7,40], which insist that perfusion MRI may efficiently capture the intratumor heterogeneity, regarding angiogenesis and vascularity of gliomas. Also, according to the literature an additive value is obtained when radiomic analysis is employed on either conventional or advanced contrast enhancement techniques [2–4,54]. However, as it has been previously reported [7] the 'hot spot' segmentation method that we utilized in CBV maps along with the subsequent inability for radiomic quantification, might have restricted the further contribution of the advanced DSCE imaging technique to the classification task.

The recent technological advancements in the field of medical imaging have given rise to the incorporation of innovative methodologies regarding tumor phenotypic characteristics quantification and multiparametric data analysis which as shown by our results may aid in improving the clinical decision support process. Besides the current technical complexity challenges of radiomic analysis, further attention should be paid in utilizing the diagnostic outcome in a reliable manner [32]. To this scope, it is evident that all methods of high-throughput analysis must consider well-established imaging techniques, which have been strongly validated upon various clinical hypotheses and underlying pathophysiology in order to guarantee their measurement accuracy and valid contribution. An equally important methodological step in such an analysis is to ensure that the involved medical personnel can ensure MR image quality, consistency and accuracy by providing minimum quality standards in the inclusion or exclusion of the evaluated radiomic parameters.

The main limitation of this study regards to the small patient sample size utilized, which possibly would have implied bias to the advanced analysis that was conducted. In addition, the sample size limitation was the main reason for the exclusion of the gliomas sub-grades differentiation task. In a future study of evaluating multiparametric MRI for glioma grade differentiation, it would be interesting to consider the inclusion of additional MR techniques with promising results (e.g. Diffusion Kurtosis Imaging, Arterial Spin Labelling). Also, except for MR modalities, an investigation of additional shape and textural radiomic features and genomic data (i.e. IDH mutation, etc) should be performed, to further assess their utility.

In conclusion, the current study presents a comprehensive methodological perspective for evaluating MRI derived phenotypic characteristics for LGG vs HGG characterization, based on multiparametric MR neuroimaging data and radiomic analysis methods. It shows that radiomic features derived from mp-MRI can be an important tool in an accurate LGG vs HGG differentiation even in this limited patient population.

Conflicts of interest

The authors declare that there is no conflict of interest regarding this research work.

Acknowledgements

We would like to thank the Wellcome/EPSRC Centre for supporting Medical Engineering [WT 203148/Z/16/Z], NIHR for funding our Biomedical Research Centre for Mental Health at the South London and Maudsley NHS Trust and the UK Research and Innovation (UKRI) for sponsoring our Data to Early Diagnosis and Precision Medicine programme.

Appendix

A. Histogram features used in the study

Min: $min_i \mathrm{p(i)}$ (A.1)

Percentile25%: $25percentile_i \mathrm{p(i)}$ (A.2)

Median: $50percentile_i \mathrm{p(i)}$ (A.3)

Percentile75%: $75percentile_i \mathrm{p(i)}$ (A.4)

Max: $max_i \mathrm{p(i)}$ (A.5)

Range: $R = max_i \mathrm{p(i)} - min_i \mathrm{p(i)}$ (A.6)

Mean: $\mu = -\sum_{i=1}^{G-1} i\mathrm{p(i)}$ (A.7)

Variance: $\sigma^2 = -\sum_{i=1}^{G-1} (i-\mu)^2 \mathrm{p(i)}$ (A.8)

$$\text{Skewness: } S = \sigma^{-3} \sum_{i=1}^{G-1} (i - \mu)^3 p(i) \tag{A.9}$$

$$\text{Kurtosis: } K = \sigma^{-4} \sum_{i=1}^{G-1} (i - \mu)^4 p(i) - 3 \tag{A.10}$$

$$\text{Entropy: } E = -\sum_{i=1}^{G-1} p(i) \log_2[p(i)] \tag{A.11}$$

$$\text{Uniformity: } U = -\sum_{i=1}^{G-1} p(i)^2 \tag{A.12}$$

where, G the number of gray levels, p(i) the approximate probability density of occurrence of the gray levels

B. GLCM features used in the study

$$\text{Angular Second Moment: } \sum_{i=1}^{Ng} \sum_{j=1}^{Ng} p(i,j)^2 \tag{B.1}$$

$$\text{Contrast: } \sum_{i=1}^{Ng} \sum_{j=1}^{Ng} (i-j)^2 p(i,j) \tag{B.2}$$

$$\text{Correlation: } \frac{\sum_{i=1}^{Ng} \sum_{j=1}^{Ng} ijp(i,j) - \mu_x \mu_y}{\rho_x \rho_y} \tag{B.3}$$

$$\text{Sum of Squares: } \sum_{i=1}^{Ng} \sum_{j=1}^{Ng} (i - \mu_x)^2 p(i,j) \tag{B.4}$$

$$\text{Inverse Difference Moment: } \sum_{i=1}^{Ng} \sum_{j=1}^{Ng} \frac{1}{1 + (i-j)^2} p(i,j) \tag{B.5}$$

$$\text{Sum Average: } \sum_{i=1}^{2Ng} i p_{(x+y)}(i) \tag{B.6}$$

$$\text{Sum Variance: } \sum_{i=1}^{2Ng} (i - SumAve)^2 p_{(x+y)}(i) \tag{B.7}$$

$$\text{Sum Entropy: } \sum_{i=1}^{2Ng} p_{(x+y)}(i) \log(p_{(x+y)}(i)) \tag{B.8}$$

$$\text{Entropy: } \sum_{i=1}^{Ng} \sum_{j=1}^{Ng} p(i,j) \log(p(i,j)) \tag{B.9}$$

$$\text{Difference Variance: } \sum_{i=1}^{Ng-1} (i - \mu_{x-y})^2 p_{(x-y)}(i) \tag{B.10}$$

$$\text{Difference Entropy: } \sum_{i=1}^{Ng} \sum_{j=1}^{Ng} p_{(x-y)}(i) \log(p_{(x-y)}(i,j)) \tag{B.11}$$

where, p(i,j) the elements of the Co-occurrence Matrix, Ng the number of gray levels, μx, μy and σx, σy denote the mean and standard deviations of the row and column sums of the GLCM, related to the marginal distributions px(i) and py(j), respectively.

C. GLRLM features used in the study

$$\text{Short Run Emphasis: } \frac{\sum_{i=1}^{Ng} \sum_{j=1}^{Nr} \frac{p(i,j)}{j^2}}{\sum_{i=1}^{Ng} \sum_{j=1}^{Nr} p(i,j)} \tag{C.1}$$

$$\text{Long Run Emphasis: } \frac{\sum_{i=1}^{Ng} \sum_{j=1}^{Nr} j^2 p(i,j)}{\sum_{i=1}^{Ng} \sum_{j=1}^{Nr} p(i,j)} \tag{C.2}$$

$$\text{Gray Level Non} - \text{Uniformity: } \frac{\sum_{i=1}^{Ng}(\sum_{j=1}^{Nr} p(i,j))^2}{\sum_{i=1}^{Ng}\sum_{j=1}^{Nr} p(i,j)} \tag{C.3}$$

$$\text{Run Length Non} - \text{Uniformity: } \frac{\sum_{j=1}^{Nr}(\sum_{i=1}^{Ng} p(i,j))^2}{\sum_{i=1}^{Ng}\sum_{j=1}^{Nr} p(i,j)} \tag{C.4}$$

$$\text{Fraction: } \frac{\sum_{i=1}^{Ng}\sum_{j=1}^{Nr} p(i,j)}{\sum_{i=1}^{Ng}\sum_{j=1}^{Nr} jp(i,j)} \tag{C.5}$$

where, p(i,j) the elements of the Run Length Matrix, Ng the number of gray levels and Nr the number of runs.

References

[1] Louis DN, Ohgaki H, Wiestler OD, Cavenee WK, Burger PC, Jouvet A, et al. WHO classification of tumours of the central nervous system. Acta Neuropathol 2007;114:97–109.

[2] Skogen K, Schulz A, Dormagen JB, Ganeshan B, Helseth E, Server A. Diagnostic performance of texture analysis on MRI in grading cerebral gliomas. Eur J Radiol 2016 Apr;85(4):824–9.

[3] Hsieha Kevin Li-Chun, Chena Cheng-Yu, Lod Chung-Ming. Quantitative glioma grading using transformed gray-scale invariant textures of MRI. Comput Biol Med 2017;1(83):102–8.

[4] Hsieh Kevin Li-Chun, Lo Chung-Ming, Hsiao Chih-Jou. Computer-aided grading of gliomas based on local and global MRI features. Comput Methods Programs Biomed 2017;139:31–8.

[5] Ryu YJ, Choi SH, Park SJ, Yun TJ, Kim JH, Sohn CH. Glioma: application of whole-tumor texture analysis of diffusion-weighted imaging for the evaluation of tumor heterogeneity. PLoS ONE 2014;30;9(9):e108335.

[6] Lee J1, Choi SH, Kim JH, Sohn CH, Lee S, Jeong J. Glioma grading using apparent diffusion coefficient map: application of histogram analysis based on automatic segmentation. NMR Biomed 2014;27(9):1046–52.

[7] Vasileios Katsaros, Katerina Nikiforaki, Giorgos Manikis, Kostas Marias, Evangelia Liouta, Christos Boskos, et al. Whole tumor MR Perfusion histogram analysis in the preoperative assessment of patients with gliomas: differentiation between high-and low-grade tumors. Hellenic J Radiol 2017;2(1).

[8] Wang Q, Zhang H, Zhang J, Wu C, Zhu W, Li F, et al. The diagnostic performance of magnetic resonance spectroscopy in differentiating high-from low-grade gliomas: a systematic review and meta-analysis. Eur Radiol 2016;26(8):2670–84.

[9] Roy Bhaswati, Gupta Rakesh K, Maudsley Andrew A, Awasthi Rishi, Sheriff Sulaiman, Meng Gu, et al. Utility of Multiparametric 3T MRI for Glioma Characterization. Neuroradiology 2013;55(5):603–13.

[10] Van Cauter S, De Keyzer F, Sima DM, Sava AC, D'Arco F, Veraart J, et al. Integrating diffusion kurtosis imaging, dynamic susceptibility-weighted contrast-enhanced MRI, and short echo time chemical shift imaging for grading gliomas. Neuro Oncol 2014;16(7):1010–21.

[11] Zacharaki EI, Wang S, Chawla S, Soo Yoo D, Wolf R, Melhem ER, et al. Classification of brain tumor type and grade using MRI texture and shape in a machine learning scheme. Magn Reson Med 2009;62(6):1609–18.

[12] Svolos P, Tsolaki E, Kapsalaki E, Theodorou K, Fountas K, Fezoulidis, et al. Investigating brain tumor differentiation with diffusion and perfusion metrics at 3T MRI using pattern recognition techniques. Magnetic Resonance Imaging 2013;31(9):1567–77.

[13] Qin Jiang-bo, Liu Zhenyu, Zhang Hui, Shen Chen, Wang Xiao-chun, Tan Yan, et al. Grading of Gliomas by Using Radiomic Features on Multiple Magnetic Resonance Imaging (MRI) Sequences. Med Sci Monit 2017;23:2168–78.

[14] Cho HH, Lee SH, Kim J, Park H. Classification of the glioma grading using radiomics analysis. PeerJ 2018;6:e5982.

[15] Zinn PO, Mahmood Z, Elbanan MG, Colen RR. Imaging Genomics in Gliomas. Cancer J. 2015;21(3):225–34.

[16] Kickingereder P, Andronesi OC. Radiomics, Metabolic, and Molecular MRI for Brain Tumors. Semin Neurol 2018;38(1):32–40.

[17] Bisdas S, Shen H, Thust S, Katsaros V, Stranjalis G, Boskos C, et al. Texture analysis-and support vector machine-assisted diffusional kurtosis imaging may allow in vivo gliomas grading and IDH-mutation status prediction: a preliminary study. Sci Rep 2018;8(1):6108.

[18] De Looze C, Beausang A, Cryan J, Loftus T, Buckley PG, Farrell M, et al. Machine learning: a useful radiological adjunct in determination of a newly diagnosed glioma's grade and IDH status. J Neurooncol 2018:16.

[19] Louis DN, Perry A, Reifenberger G, von Deimling A, Figarella-Branger D, Cavenee WK, et al. The 2016 World Health Organization Classification of Tumors of the Central Nervous System: a summary. Acta Neuropathol. 2016;131(6):803–20.

[20] Citak-Er Fusun, Firatc Zeynep, Kovanlikayad Ilhami, Turee Ugur, Ozturk-Isikf Esin. Machine-learning in grading of gliomas based on multi-parametric magnetic resonance imaging at 3T. Comput Biol Med 2018;1(99):154–60.

[21] Tian Q, Yan LF, Zhang X, Zhang X, Hu YC, Han Y, et al. Radiomics strategy for glioma grading using texture features from multiparametric MRI. J Magn Reson Imaging 2018;48(6):1518–28.

[22] Wilson M, Reynolds G, Kauppinen RA, Arvanitis TN, Peet AC. A constrained least-squares approach to the automated quantitation of in vivo 1H magnetic resonance spectroscopy data. Magn Reson Med 2011;65(1):1–12.

[23] Boxerman JL, Prah DE, Paulson ES, Machan JT, Bedekar D, Schmainda KM. The Role of preload and leakage correction in gadolinium-based cerebral blood volume estimation determined by comparison with MION as a criterion standard. AJNR Am J Neuroradiol 2012;33(6):1081–7.

[24] Bjornerud A, Sorensen AG, Mouridsen K, Emblem KE. T1- and T*2-Dominant Extravasation Correction in DSC-MRI: Part I—Theoretical Considerations and Implications for Assessment of Tumor Hemodynamic Properties. J Cereb Blood Flow Metab 2011;31(10):2041–53.

[25] Welker K, Boxerman J, Kalnin A, Kaufmann T, Shiroishi M, Wintermark M. ASFNR Recommendations for Clinical Performance of MR Dynamic Susceptibility Contrast Perfusion Imaging of the Brain. Am J Neuroradiol 2015;36(6).

[26] Jenkinson M, Beckmann CF, Behrens TE, Woolrich MW, Smith SM. FSL NeuroImage 2012;62:782–90.

[27] Jenkinson M, Smith SM. A global optimisation method for robust affine registration of brain images. Med Image Anal 2001;5(2):143–56.

[28] Jenkinson M, Bannister PR, Brady JM, Smith SM. Improved optimisation for the robust and accurate linear registration and motion correction of brain images. NeuroImage 2002;17(2):825–41.

[29] Andersson Jesper LR, Sotiropoulos Stamatios N. An integrated approach to correction for off-resonance effects and subject movement in diffusion MR imaging. NeuroImage 2016;125:1063–78.

[30] Smith SM, Jenkinson M, Woolrich MW, Beckmann CF, Behrens TEJ, Johansen-Berg H, et al. Advances in functional and structural MR image analysis and implementation as FSL. NeuroImage 2004;23(S1):208–19.

[31] Vamvakas A, Tsougos I, Arikidis N, Kapsalaki E, Fountas K, Fezoulidis et al. Exploiting morphology and texture of 3D tumor models in DTI for differentiating glioblastoma multiforme from solitary metastasis. Biomed Signal Process Control 43;159–173.

[32] Napel S, Mu W, Jardim-Perassi BV, Aerts HJWL, Gillies RJ. Quantitative imaging of cancer in the postgenomic era: Radio(geno)mics, deep learning, and habitats. Cancer 2018:1.

[33] Scarabino T, Popolizio T, Trojsi F, Giannatempo G, Pollice S, Maggialetti N, et al. Role of advanced MR imaging modalities in diagnosing cerebral gliomas. Radiol Med 2009;114(3):448–60.

[34] Server A, Josefsen R, Kulle B, Maehlen J, Schellhorn T, Gadmar O et al. Proton magnetic resonance spectroscopy in the distinction of high-grade cerebral gliomas from single metastatic brain tumors. Acta Radiol 51(3);316–325.

[35] Tsougos I. Advanced MR Neuroimaging: From Theory to Clinical Practice. Boca Raton, FL, USA: CRC Press; 2017.

[36] Weber MA, Zoubaa S, Schlieter M, Juttler E, Huttner HB, Geletneky K, et al. Diagnostic performance of spectroscopic and perfusion MRI for distinction of brain tumors. Neurology 2006;66(12):1899–906.

[37] Chawla S, Zhang Y, Wang S, et al. Proton magnetic resonance spectroscopy in differentiating glioblastomas from primary cerebral lymphomas and brain metastases. J Comput Assist Tomogr 2010;34(6):836–41.

[38] Materka M. Strzelecki. 1998. Texture Analysis Methods – A Review, Technical University of Lodz, Institute of Electronics, COST B11 report, Brussels.

[39] Strzelecki M, Szczypinski P, Materka A, Klepaczko A. A software tool for automatic classification and segmentation of 2D/3D medical images. Nucl Instruments Methods Phys Res A 2013;702:137–40.

[40] Szczypinski P, Strzelecki M, Materka A, Klepaczko A. MaZda-A software package for image texture analysis. Comput Methods Programs Biomed 2009;94(1):66–76.

[41] Zhang X, Yan LF, Hu YC, Li G, Yang Y, Han Y, et al. Optimizing a machine learning based glioma grading system using multi-parametric MRI histogram and texture features. Oncotarget 2017;8(29):47816–30.

[42] Eibe Frank, Mark A Hall, Ian H Witten. The WEKA Workbench. 2016. Online Appendix for "Data Mining: Practical Machine Learning Tools and Techniques", Morgan Kaufmann, Fourth Edition.

[43] Guyon I, Weston J, Barnhill S, Vapnik V. Gene Selection for Cancer Classification using Support Vector Machines. Mach Learn 2002;46:389.

[44] Platt JC, Nitschke RV. Sequential minimal optimization: a fast Algorithm for Training Support Vector machines. Technical Report 1998. MSR-TR-98-14.

[45] Chen Wei, Liu Boqiang, Peng Suting, Sun Jiawei, Qiao Xu. Computer-Aided Grading of Gliomas Combining Automatic Segmentation and Radiomics. Int J Biomed Imaging 2018.

[46] Geethu Mohan M. Monica Subashini, MRI based medical image analysis: survey on

brain tumor grade classification. Biomed Signal Process Control January 2018;39:139–61.
[47] Parekh V, Jacobs MA. Radiomics: a new application from established techniques. Expert Rev Precis Med Drug Dev. 2016;1(2):207–26.
[48] Server A, Kulle B, Gadmar ØB, Josefsen R, Kumar T. Nakstad PH., Measurements of diagnostic examination performance using quantitative apparent diffusion coefficient and proton MR spectroscopic imaging in the preoperative evaluation of tumor grade in cerebral gliomas. Eur J Radiol 2011;80(2):462–70.
[49] Wang S, Meng M, Zhang X, Wu C, Wang R, Wu J, et al. Texture analysis of diffusion weighted imaging for the evaluation of glioma heterogeneity based on different regions of interest. Oncol Lett. 2018;15(5):7297–304.
[50] Brynolfsson P, Nilsson D, Henriksson R, Hauksson J, Karlsson M, Garpebring A, et al. ADC texture–an imaging biomarker for high-grade glioma? Med Phys 2014;41(10):101903.
[51] Raja R, Sinha N, Saini J, Mahadevan A, Rao KN, Swaminathan A. Assessment of tissue heterogeneity using diffusion tensor and diffusion kurtosis imaging for grading gliomas. Neuroradiology 2016;58(12):1217–31.
[52] Kousi E, Tsougos I, Tsolaki E, Fountas KN, Theodorou K, Fezoulidis I, et al. Spectroscopic evaluation of glioma grading at 3T: the combined role of short and long TE. Scientific World J 2012;2012.
[53] Tsougos I, Svolos P, Kousi E, Fountas K, Theodorou K, Fezoulidis I, et al. Differentiation of glioblastoma multiforme from metastatic brain tumor using proton magnetic resonance spectroscopy, diffusion and perfusion metrics at 3 T. Cancer Imaging 2012;12(3):423.
[54] Su CQ, Lu SS, Han QY, Zhou MD, Hong XN. Intergrating conventional MRI, texture analysis of dynamic contrast-enhanced MRI, and susceptibility weighted imaging for glioma grading. Acta Radiol 2018;23. 284185118801127.
[55] Court Laurence E, Fave Xenia, Mackin Dennis, Lee Joonsang, Yang Jinzhong, Zhang Lifei. Computational resources for radiomics. Transl Cancer Res 2016;5(4):340–8.